Journal of Ceramic Processing Research. Vol. 26, No. 4, pp. 606~617 (2025)
(Received 26 May 2025, Received in revised form 10 June 2025, Accepted 11 June 2025)
https://doi.org/10.36410/jcpr.2025.26.4.606

J O U R N A L O F
Ceramic Processing Research

Valorization of wastewater sludge into carbon materials for energy storage applications: feasibility and economic assessment

Saehee Lee[a], Chanwoo Kim[a], Uijun Lee[b], Hyeonmin Jo[a], Hee-Dae Lim[a,b,*] and Byoung-In Sang[a,c,*]
[a]*Department of Chemical Engineering, Hanyang University, 222 Wangsimni-ro, Seongdong-gu, Seoul 04763, Republic of Korea*
[b]*Department of Battery Engineering, Hanyang University, 222 Wangsimni-ro, Seongdong-gu, Seoul 04763, Republic of Korea*
[c]*Clean-Energy Research Institute, Hanyang University, 222 Wangsimni-ro, Seongdong- gu, Seoul 04763, Republic of Korea*

The increasing accumulation of sewage sludge from wastewater treatment presents both environmental and economic concerns. This study proposes a sustainable valorization approach by converting sludge into porous carbon materials for lithium metal battery applications. Sludge underwent chemical pretreatment, pyrolysis at 800 °C, and KOH activation to yield carbon (Sludge C) with tailored structure and functionality. Physicochemical characterization confirmed a microporous structure, oxygen-rich surface groups, and partial crystallinity due to residual inorganic elements such as Si, Al, and Fe. Compared to commercial Super P, Sludge C exhibited lower lithium nucleation overpotential and improved cycling stability, attributed to its lithiophilic species and high surface area. A techno-economic analysis compared sludge carbonization with incineration, composting, and biohydrogen production. Despite higher capital costs, sludge carbonization offered promising value recovery through electrode material production. This study highlights a scalable and eco-friendly pathway for transforming sewage sludge into functional materials for energy storage, supporting waste minimization and circular bioeconomy goals.

Keywords: Sewage sludge valorization, Sludge-derived carbon, Lithiophilic interlayer, Techno-economic analysis.

Introduction

The global increase in wastewater production has resulted in the large-scale generation of sewage sludge, a byproduct of municipal and industrial wastewater treatment [1]. Traditionally, sludge has been managed through energy-intensive processes such as incineration, landfilling, or composting, all of which pose environmental concerns and incur substantial operational costs [2]. Due to its rich composition of organic and inorganic substances, sewage sludge is increasingly considered a promising yet underexploited feedstock for the synthesis of carbon-based materials. Recent studies have explored the thermochemical conversion of biomass and waste-derived feedstocks into functional carbon materials for energy storage applications [3, 4]. Among these, sewage sludge has gained attention due to its low cost, abundant availability, and inherent composition of carbon precursors and catalytically active inorganics. When subjected to carbonization and chemical activation, sludge can yield porous carbon structures [5] with electrochemically active surfaces suitable for integration in energy storage devices. Despite these promising attributes, sludge-derived carbon (SDC) is typically characterized by low purity, disordered structure, and compositional heterogeneity due to residual metal oxides and coagulant-derived species [6]. These features are seen as limitations in comparison to commercial carbon additives such as carbon black, carbon nanotubes (CNTs), and graphene. However, these same characteristics—such as the presence of lithiophilic metals (e.g., Si, Al, Mg)—may offer unique advantages when SDC is used as a current collector coating or interlayer in next-generation lithium metal batteries (LMBs), particularly in the development of anode-free lithium metal batteries (AFLMBs).

In parallel with technical feasibility, economic viability remains a critical aspect for commercial implementation. While high-performance carbon nanomaterials offer superior electrochemical characteristics, the energy storage industry continues to face critical challenges associated with high production costs and constrained material availability [7]. In contrast, SDC offers a low-cost and potentially sustainable alternative, especially if produced from waste streams that would otherwise require disposal.

In this study, we report a comprehensive assessment of carbon materials derived from sewage sludge obtained from a municipal wastewater treatment plant. The sludge was subjected to acid washing, pyrolysis, and chemical activation to produce carbon materials with tailored porosity and surface functionality. The prepared SDC was structurally and electrochemically compared with Super P, a standard conductive carbon. Furthermore, its

*Co-corresponding author
Professor Hee-Dae Lim
Tel. +82-2-2220-0531; E-mail: hdlim@hanyang.ac.kr
Professor Byoung-In Sang
Tel. +82-2-2220-2328; E-mail: biosang@hanyang.ac.kr

application as a current collector coating in lithium metal batteries was evaluated, accompanied by a comprehensive techno-economic analysis comparing alternative sludge valorization strategies. This work demonstrates the dual environmental and economic benefits of converting wastewater sludge into functional energy materials, supporting the broader transition toward a circular and sustainable bioeconomy.

Materials and Methods

Sludge pretreatment

Sludge cake (350.12 g), obtained from the aeration tank of the Jungnang wastewater treatment plant (Seoul, Republic of Korea), was dispersed in distilled water and homogenized thoroughly. The mixture was centrifuged at 4,000 rpm for 5 min to remove soluble impurities, and the supernatant was discarded. The sludge was washed with distilled water, and this process was repeated three times. To eliminate residual coagulants, the washed sludge was treated with 10% hydrochloric acid (HCl) at a solid-to-liquid ratio of 1:2 (w/v) and stirred for 2 h at room temperature. After acid treatment, the mixture was centrifuged at 4,000 rpm for 5 min and the supernatant was discarded. The precipitate was washed with distilled water six times, and the pH was adjusted to neutral by a NaOH solution. The resulting sample was freeze-dried at –60 °C for 24 h and stored for subsequent carbonization.

Preparation and processing of sludge-derived carbon materials

The freeze-dried sludge samples were carbonized in a tubular furnace under an argon (Ar) atmosphere. The temperature was increased from room temperature to 800 °C at a heating rate of 5 °C min^{-1}, and maintained at 800 °C for 2 h. The resulting carbon materials were collected and subjected to acid leaching to remove residual metal components. Specifically, 1.5 g of carbon was mixed with 90 mL of 6 M H_2SO_4 (equivalent to approximately 3.3 g H_2SO_4 per gram of carbon) and stirred overnight at room temperature. After acid treatment, the suspension was vacuum-filtered using a PVDF hydrophilic membrane (47 mm diameter, 0.22 μm pore size), and thoroughly washed with distilled water until neutral pH was achieved. The filtered solid was dried in an oven at 60 °C overnight. Subsequently, chemical activation was carried out by mixing the acid-treated carbon with 0.1 M KOH and heating the mixture at 800 °C for 1 h. The mass ratio of KOH to carbon was maintained at 3:1. After activation, the samples were dried and ground into a fine powder for further use. The overall mass yield of sludge-derived carbon after pyrolysis and KOH activation was approximately 41% based on the dry sludge input.

Physicochemical characterization of carbon materials

The morphological and structural properties of the carbon materials obtained from wastewater sludge were characterized and compared to commercial Super P carbon (TIMCAL, Switzerland). Surface morphology was examined using scanning electron microscopy (Cryo FIB-SEM; Crossbeam550, ZEISS, Germany, NFEC-2025-03-304629) at an accelerating voltage of 15 kV. Prior to imaging, the samples were sputter-coated with platinum. The internal microstructure of the sludge-derived carbon was further analyzed by transmission electron microscopy (TEM; JEM-2100F, JEOL, Japan). Samples were dispersed in ethanol, ultrasonicated, and drop-cast onto carbon-coated copper grids. High-resolution TEM imaging was conducted along with selected area electron diffraction (SAED), fast Fourier transform (FFT), and energy-dispersive X-ray spectroscopy (EDS) analysis to investigate crystallinity and elemental distribution at the nanoscale. X-ray diffraction (XRD; D8 ADVANCE, Bruker, Germany) was conducted to evaluate the crystalline structure of the carbon materials, with scans recorded from 5° to 60° (2θ) at a step size of 0.05°. Raman spectroscopy (DXR-3xi, Thermo Fisher Scientific, USA) was employed to assess the degree of graphitization and structural disorder by analyzing the D- and G-bands. Fourier transform infrared spectroscopy (FTIR; Cary 630, Agilent Technologies, USA) was used to identify functional groups on the surface of the carbon materials in the wavenumber range of 4,000~400 cm^{-1} using the attenuated total reflectance (ATR) mode. X-ray photoelectron spectroscopy (XPS; K-Alpha+, Thermo Fisher Scientific, USA) was performed to determine the surface chemical composition and bonding states of carbon, oxygen, and other elements. Nitrogen adsorption and desorption isotherms were measured at 77 K using a BET surface area analyzer (ASAP 2460M, Micromeritics, USA) to evaluate the specific surface area and pore size distribution of the samples.

Electrochemical evaluation of carbon materials

Polyvinylidene fluoride (PVDF) and N-methyl-pyrrolidone (NMP) were purchased from Sigma Aldrich. Li metal foil and polyethylene separator were obtained fromWellcos and ACEY, respectively. The electrolyte purchased from Dongwha Co. consisted of 1 M lithium hexafluorophosphate ($LiPF_6$) dissolved in ethylene carbonate (EC), dimethylcarbonate (DMC), and fluoroethylene carbonate (FEC) at a volume ratio of 45:45:10. To prepare the sludge carbon electrode, sludge-derived carbon and PVDF were mixed in an NMP at a ratio of 9:1 using a Thinky planetary mixer. The resulting slurry was cast onto Cu foil with a loading level of 7.96 mg cm^{-2}. The prepared electrodes were dried at 80 °C and vacuumed for 12 h. The Super P electrodes were prepared using the same method and composition. Electrochemical performance was tested using CR2032 coin-type cells, which were assembled in an argon-filled glove box (<0.1 ppm of O_2 and H_2O). For the half-cell test, each substrate and a Li foil were used

as the working electrode and the counter, respectively. A polyethylene (PE) separator and 100 μL of electrolyte were used for each cell. Prior to testing, the cells were rested for 12 h and pre-cycled for three formation cycles at 0.1 mA cm^{-2} with a capacity of 1 mAh cm^{-2}. Galvanostatic charge–discharge cyclings were performed using a battery cycler (Neware, MIHW-200-160CH-B).

Techno-Economic analysis

Base design of process

The techno-economic evaluation was performed using SuperPro Designer® (v.12, Intelligen, Inc., Scotch Plains, NJ, USA), based on a processing capacity of 1.59 million tons per day, which corresponds to the influent treatment capacity of the Jungnang Wastewater Treatment Plant located in Seoul, South Korea. The base case was defined as the process from raw sludge to sludge cake, including aerobic digestion, sedimentation, solid concentration via belt filtration, and the final drying to produce the sludge cake (Fig. 1). A process flowsheet for sludge cake production is presented below. The influent flow was composed of domwaste, fixed suspended solids, nitrate, water, X-vss-h, X-vss-n, X-vss-I, and total dissolved solids [8]. In the two-stage aerobic digestion process, the following biochemical reactions were modeled: Domwaste degradation, nitrification, X-vss-h, and X-vss-n decay. The corresponding stoichiometric reactions are as follows:

$$0.1\ NH_3 + 1.0\ DomWaste + 1.4\ O_2 \rightarrow 0.9\ CO_2 + 0.8\ H_2O + 0.8\ X_{vss-h} \quad (1)$$

$$7.5\ NH_3 + 1.8\ CO_2 + 24.6\ O_2 \rightarrow 25.2\ NO_3 + 7.7\ H_2O + 1.0\ X_{vss-n} \quad (2)$$

$$1.15\ O_2 + 1.05\ X_{vss-h} \rightarrow 0.1\ NH_3 + 1.45\ CO_2 + 0.45\ H_2O + 0.20\ X_{vss-i} \quad (3)$$

$$1.15\ O_2 + 1.05\ X_{vss-n} \rightarrow 0.1\ NH_3 + 1.45\ CO_2 + 0.45\ H_2O + 0.20\ X_{vss-i} \quad (4)$$

Case study of various uses for sludge cake

Sludge cake can be utilized in various ways. In this study, a techno-economic evaluation was conducted for four different treatment pathways: incineration, composting, biohydrogen production, and carbonization of sludge—based on the specific characteristics of the sludge used in our experiments [9, 10]. For incineration, sludge cake with a moisture content of 65% was combusted at high temperatures in the presence of auxiliary fuel. The process considered in this evaluation involves direct thermal combustion without energy recovery systems. In the case of composting, due to the low carbon content of the sludge, supplemental carbon sources such as lignin or cellulose were added to facilitate aerobic degradation. The moisture content was adjusted to 50%, and the operating temperature was maintained at 60 °C. During aerobic digestion, carbon sources are broken down into glucose, and the following reaction occurs:

$$1\ Glucose + 6\ O_2 \rightarrow 6\ CO_2 + 6\ H_2O + Heat \quad (5)$$

The heat generated from this reaction was considered as recoverable energy, and the final composted material was treated as a value-added fertilizer product, revenue.

For biohydrogen production, the sludge stream—prior to the drying step—was supplemented with carbon sources and subjected to anaerobic fermentation to produce hydrogen-rich biogas. The representative metabolic pathways for fermentation are as follows [11]:

$$C_6H_{12}O_6 + 2\ H_2O \rightarrow 2\ CH_3COOH + 2\ CO_2 + 4\ H_2 \quad (6)$$

$$C_6H_{12}O_6 \rightarrow CH_3CH_2CH_2COOH + 2\ CO_2 + 2\ H_2 \quad (7)$$

To purify the produced hydrogen gas, condensation and desulfurization processes were incorporated to remove water vapor and corrosive hydrogen sulfide, respectively. Subsequently, pressure swing adsorption (PSA) was used to obtain high purity biohydrogen [12].

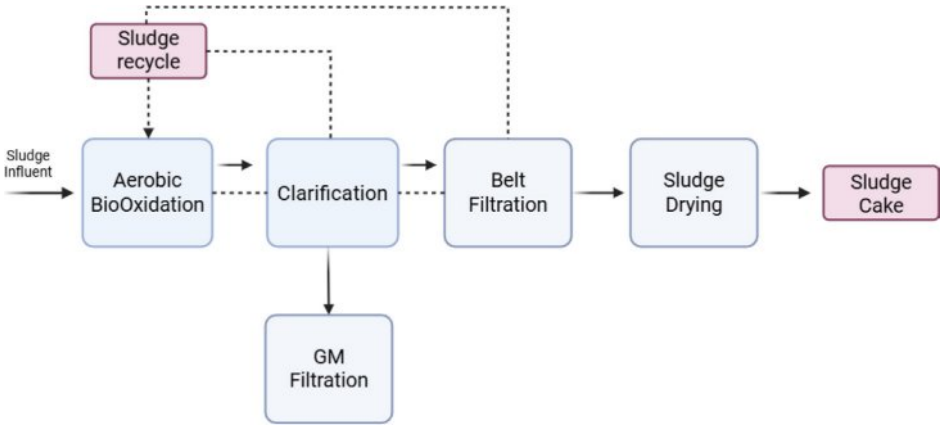

Fig. 1. Schematic diagram of producing sludge cake.

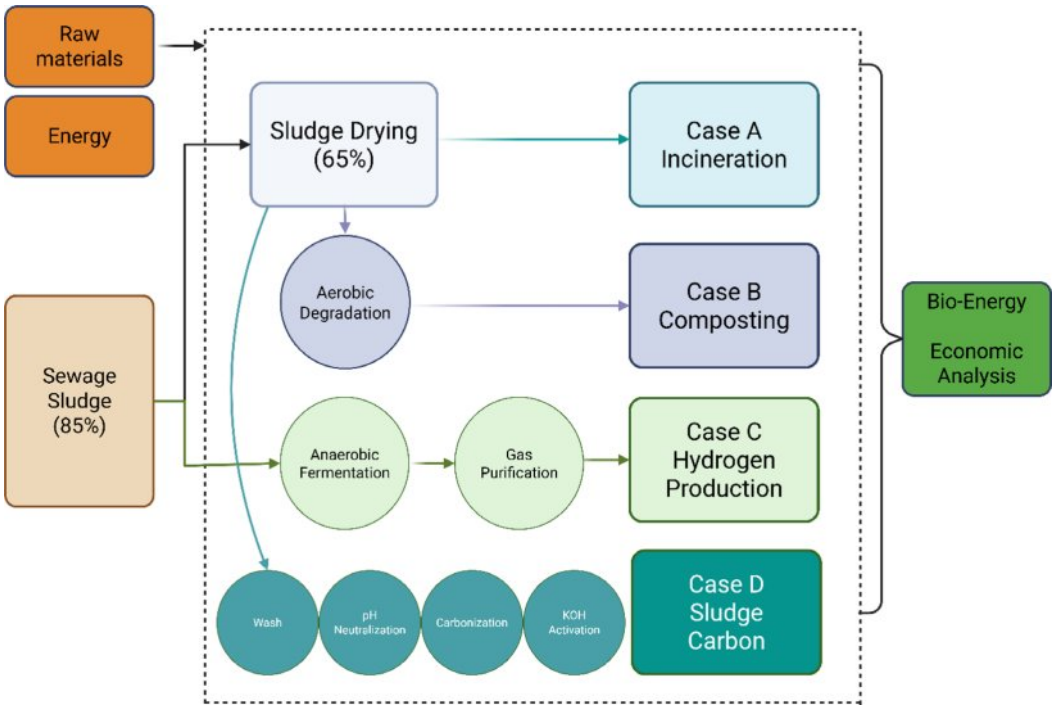

Fig. 2. Case study on various uses of sludge.

For storage, the purified gas was liquefied and stored under high pressure. The energy content of biohydrogen was assessed based on its lower heating value (LHV).

In our experimental case, the sludge cake was initially washed with tap water to remove surface impurities, followed by pretreatment with 10% HCl to eliminate trace metals. The pH was then neutralized using NaOH. Complete moisture removal was achieved through belt filtration and subsequent drying. The resulting dried sludge was carbonized at 800 °C to produce sludge-derived carbon. Finally, chemical activation using 0.1 M KOH was carried out to enhance the material's properties for potential application as a battery material. These processes are shown in Fig. 2. Key assumptions for the simulation include a 30-month construction period, a 15-year project lifetime, and 330 operating days per year. The Net Present Value (NPV) interest rates were categorized as low (7%), medium (9%), and high (11%), with a depreciation period of 10 years calculated using the straight-line method at 5%. The inflation rate was set at 4.00%. The prices of raw materials were detailed in Table 1, along with a summary of the material flow and product yields during the process. These parameters provided the foundation for the economic analysis and comparison of the different process configurations.

Table 1. Market price of raw materials.

	Items	UNIT COST
	Materials	
Carbon source	Lignin	$ 0.15 / kg
	Hemicellulose	$ 0.37 / kg
	Glucose	$ 0.59 / kg
Coagulant	Polymer	$ 2.25 / kg
Raw materials	Water	$0.0007 / L
	Fuel	$ 0.85 / L
	10% HCl (aq)	$ 0.11 / L
	10% NaOH (aq)	$ 0.074 / L
Revenue	Sludge influent	$ 1 / Mton
	Biohydrogen	$ 1.5 / kg
	Compost	$ 58.72 / ton

Results and Discussion

Morphological and elemental analysis

The morphological characteristics of Super P and sludge-derived carbon (Sludge C) were examined using SEM and TEM. As shown in Fig. 3, Super P exhibited uniform, spherical particles with clean and smooth surfaces, indicative of high structural uniformity. In contrast, Sludge C displayed irregular shapes, agglomerated structures, and a wrinkled texture. These morphological differences are attributed to the nature of the sludge precursor and the presence of residual inorganic components. Further insights into internal structure were obtained through TEM analysis (Fig. 4a, b). Super P demonstrated well-defined concentric graphitic layers, while Sludge C showed largely amorphous morphology with fragmented carbon domains. Selected area electron

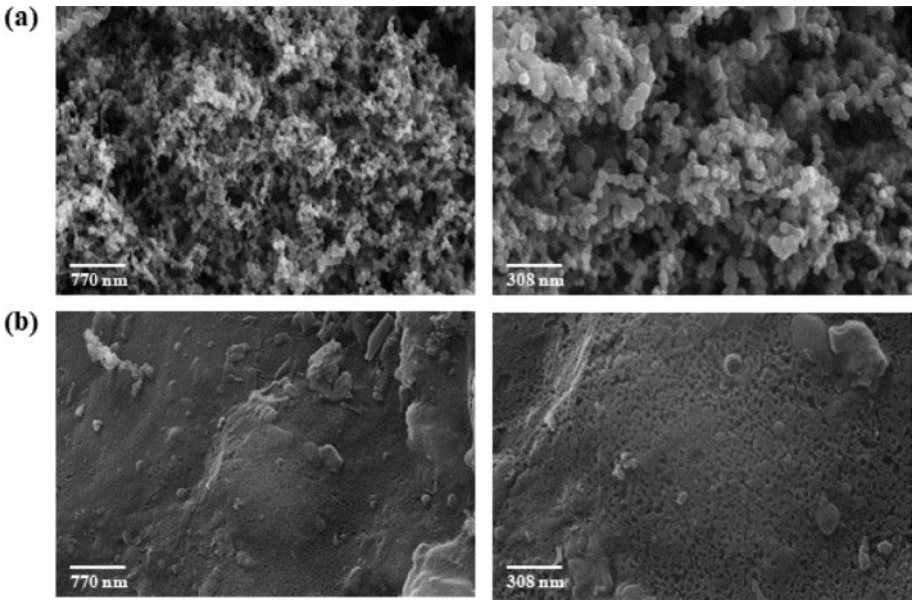

Fig. 3. SEM of (a) Super P and (b) sludge-derived carbon.

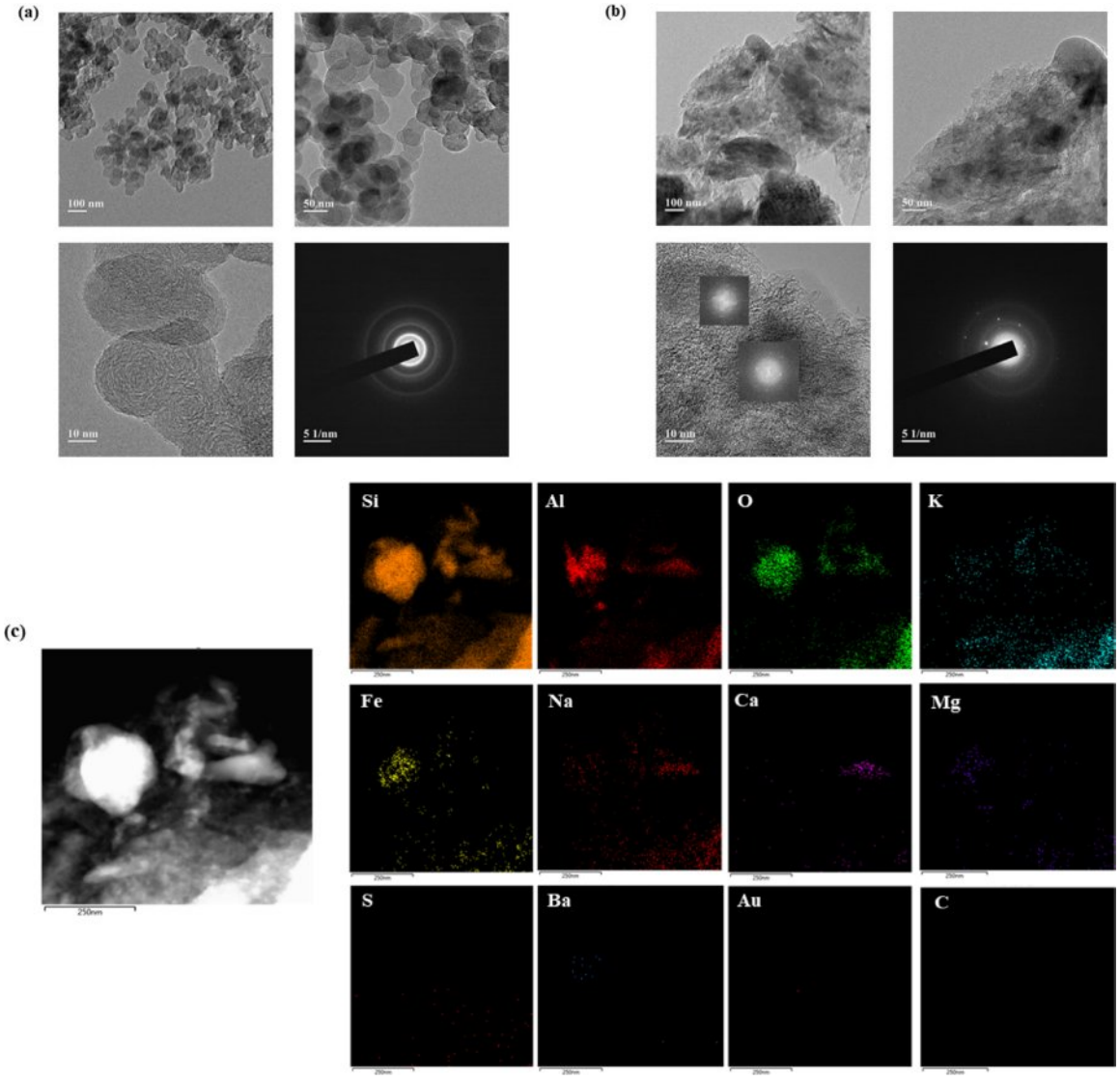

Fig. 4. TEM images of (a) Super P and (b) sludge-derived carbon, and (c) EDS mapping of sludge carbon.

diffraction (SAED) patterns and FFT analysis confirmed the partially crystalline nature of Sludge C. EDS mapping (Fig. 4c) revealed that, unlike the pure carbon composition of Super P, Sludge C contained various inorganic elements such as Si, Al, Fe, and Ca, consistent with its origin from sewage treatment processes. Therefore, it is inferred that the crystalline features observed in Sludge C originate mainly from embedded inorganic constituents rather than from intrinsic graphitization.

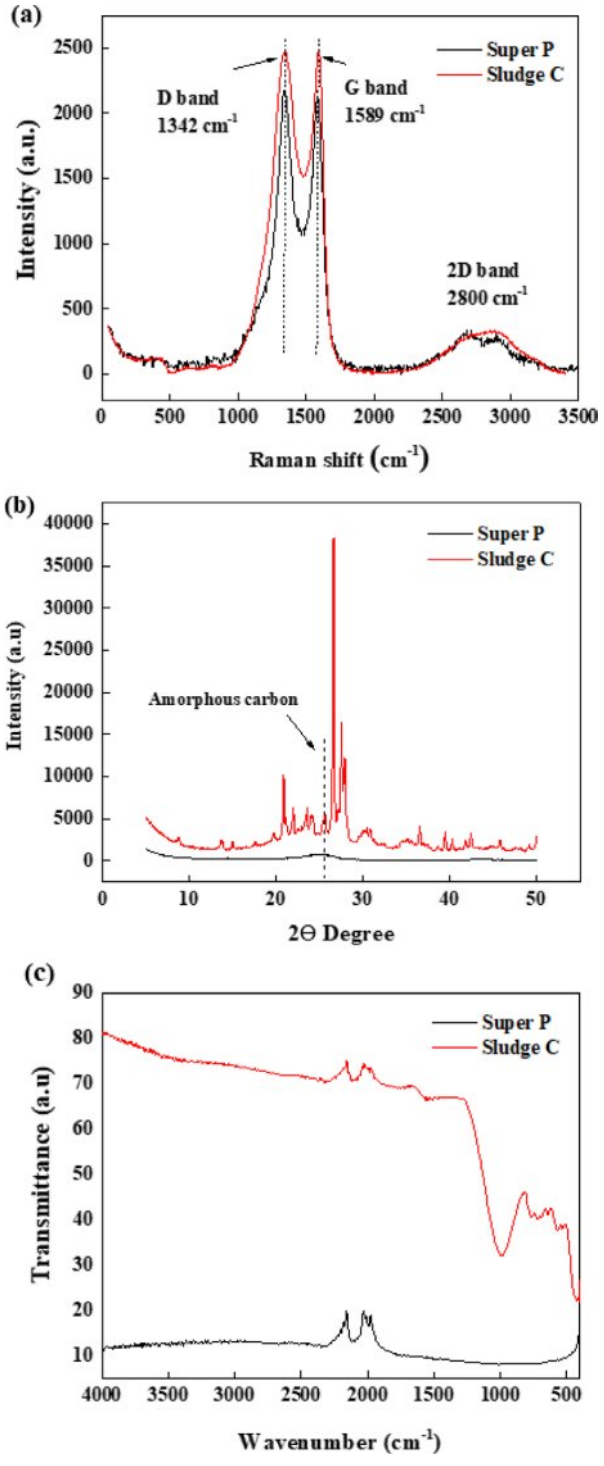

Fig. 5. (a) Raman spectra, (b) XRD patterns, and (c) FTIR spectra of Super P and sludge carbon.

Structural and chemical properties

The structural features observed in TEM were further investigated using Raman spectroscopy, XRD, and FTIR (Fig. 5). In the Raman spectra (Fig. 5a), the D-band at 1,342 cm^{-1} and G-band at 1,589 cm^{-1} were evident in both samples. The ID/IG ratio of the sludge-derived carbon was comparable to that of Super P, suggesting a similar level of structural disorder and degree of graphitization. XRD patterns (Fig. 5b) further supported this observation by showing that Super P exhibited a sharp and well-defined (002) diffraction peak typical of graphitic carbon, while Sludge C exhibited a broad peak around 24, typical of disordered carbon with low graphitization [13]. Additionally, multiple sharp diffraction peaks were observed across the full scan range, which are attributed to residual inorganic components such as Si-, Al-, and Fe-based oxides originating from the sludge matrix [14]. These results confirm that the apparent crystallinity in Sludge C primarily arises from mineral residues rather than carbon lattice ordering. The FT-IR spectra of Sludge C (Fig. 5c) exhibited distinct absorption bands at ~3,400 cm^{-1}, ~1,700 cm^{-1}, and ~1,100 cm^{-1}, corresponding to O–H, C=O, and C–O stretching vibrations, respectively [15]. These features indicate the presence of surface hydroxyl, carbonyl, and ether groups, likely introduced during chemical pretreatment. In contrast, Super P showed minimal functional group signals, reflecting its high purity and low surface reactivity. The enriched surface chemistry of Sludge C may affect its interfacial behavior in electrochemical systems.

Surface area and elemental composition

The differences in microstructure and surface chemistry were reflected in nitrogen adsorption-desorption isotherms and XPS results (Fig. 6). The N_2 adsorption–desorption isotherms (Fig. 6a) indicated a higher surface area for Sludge C compared to Super P, with the former exhibiting a more gradual uptake and a nearly hysteresis-free profile, suggestive of a microporous structure. BJH pore distribution analysis (Fig. 6a) further revealed that Sludge C primarily contained pores below 10 nm, while Super P showed a broad mesopore distribution centered around 40 nm. These structural differences suggest that Sludge C provides a higher interfacial area but potentially limited ion transport under high-rate conditions. Moreover, the BET surface area of sludge derived carbon was higher (82.8 m^2 g^{-1}) than that of Super P (58.8 m^2 g^{-1}), although its total pore volume was smaller (0.06 vs. 0.23 cm^3 g^{-1}), and average pore diameter was significantly reduced (3.28 nm vs. 14.18 nm). This indicates a transition to microporous structure, which can enhance ion-accessible surface but may limit electrolyte transport at high current densities. The XPS survey spectrum (Fig. 6b) of Sludge C confirmed the presence of multiple elements including C, O, and residual

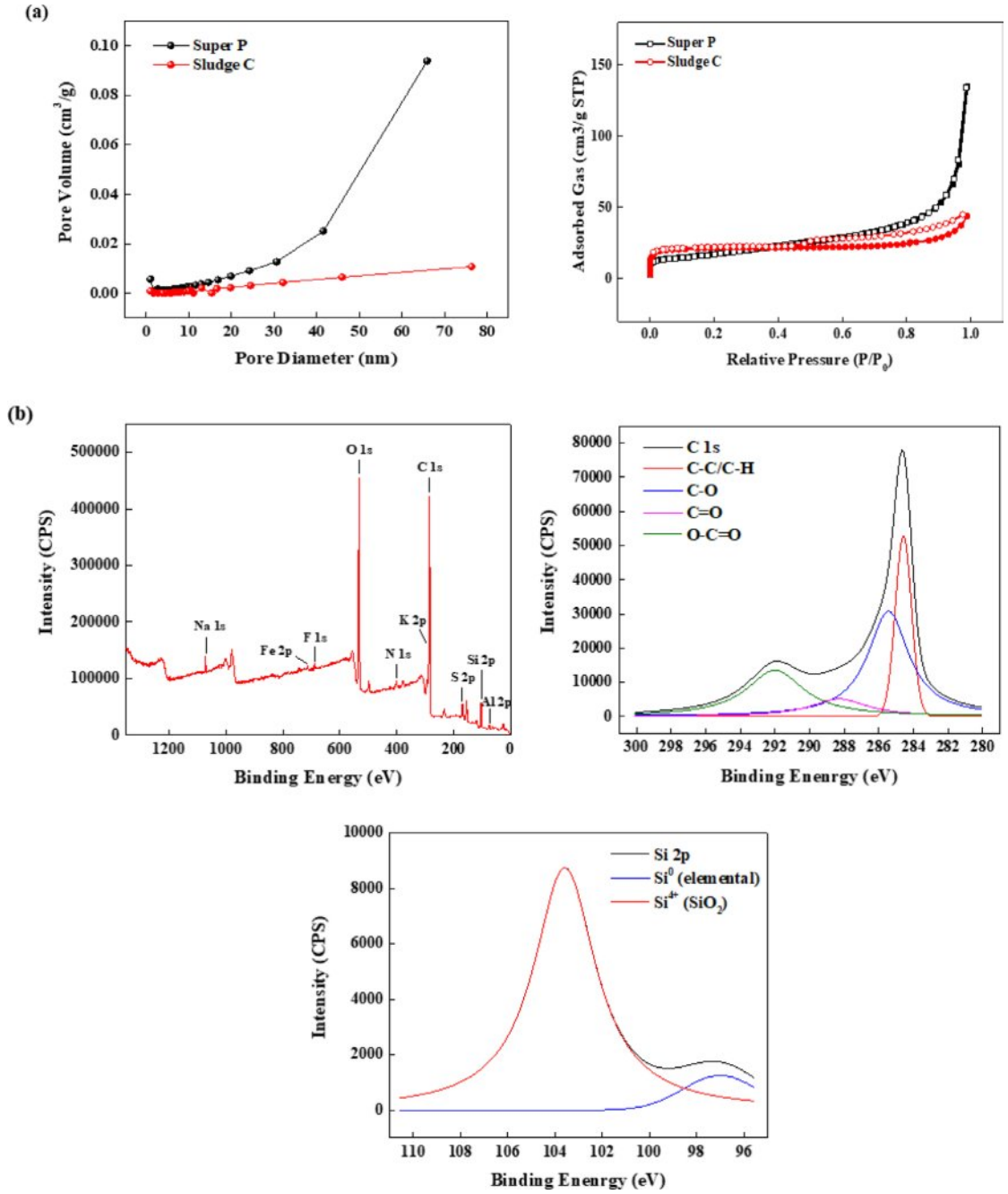

Fig. 6. (a) N_2 adsorption–desorption isotherms and pore distribution curves; (b) XPS survey and high-resolution spectra of sludge carbon, showing C 1s and Si 2p bonding environments.

inorganics such as Si, Al, and Fe. High-resolution C 1s spectra showed characteristic peaks at 284.8, 286.2, 287.6, and 289.0 eV, corresponding to C–C, C–O, C=O, and O–C=O groups, respectively [16]. These indicate the presence of oxygen-rich functional groups on the carbon surface, which may affect electrolyte interaction and SEI formation. The Si 2p spectrum revealed both elemental silicon (Si^0) and oxidized silicon (Si^{4+}) [17], suggesting that the observed crystallinity in XRD patterns is largely due to residual silicate-based minerals from the sludge matrix rather than carbon lattice ordering.

Potential of sludge carbon as anode-free lithium metal batteries current collector

Due to the emergence of electric vehicles, next-generation battery systems with high energy densities than conventional lithium-ion batteries (LIBs) are gaining significant attention. Among these, lithium metal batteries (LMBs), which utilize lithium metal as the anode, are regarded as one of the most promising candidate due to the lowest electrical potential of lithium (-3.04 V *vs.* SHE) and high specific capacity (3,862 mAh g^{-1}) [18-20]. However, despite these significant

advantages, the practical energy density of LMBs is often compromised by the employment of an excess lithium metal on the anode side [21]. To address this, recent research focused on minimizing lithium usage, with the goal being the complete elimination of excess lithium metal on the anode side, so-called anode-free lithium metal batteries (AFLMBs) [21-23]. Although AFLMBs can theoretically deliver the highest energy density on the anode side, several challenges make it less favorable to the practical application compared to the LMBs or commercial graphite anodes. Among the various problems, inhomogeneous lithium plating and stripping behaviors, which lead to dendrite growth, are particularly problematic. The dendrites trigger continuous side reactions, cause huge volume changes during cycling and cell short circuits, finally resulting in rapid battery failure and safety concerns [24, 25]. In this context, strategies for designing three-dimensional current collectors (3DCC) have recently been proposed to mitigate dendrite growth by reducing local current density [26, 27]. Various metal-based 3DCCs such as Cu and Ni have been investigated for this purpose, however, these heavy frames inherently compromise the gravimetric energy density of the overall system [21, 28].

Consequently, electrically conductive carbon materials such as amorphous carbon, graphene, and carbon nanotubes (CNTs) have been explored as alternative 3DCCs [29-31]. Unfortunately, these carbon materials have high production costs and face limitations in the large-scale fabrication of carbon-based electrodes. Additionally, most of these carbon hosts suffer from poor lithiophilicity and wettability with electrolytes, which result in inhomogeneous lithium deposition [32, 33]. In contrast to conventional conductive carbon materials, sludge carbon inherently contains metallic species such as Si, Al, and Mg that exhibit lithiophilic behavior [34, 35], thereby promoting uniform lithium nucleation and growth. In addition, the large specific surface area and high electrical conductivity of sludge carbon effectively disperse the applied current, thereby facilitating uniform lithium deposition. Further, we verified the lithiophilicity of sludge carbon, as shown in Fig. 7. Bare Cu, Super P, and sludge carbon substrate were prepared, and comparison of nucleation overpotential was performed on each substrate. As shown in Fig. 7a, the nucleation overpotential for lithium deposition was significantly reduced on the sludge carbon (KOH) electrode (8.7 mV) compared to Super P (17.3 mV) and bare Cu (38.5 mV), which can be attributed to the effective current dispersion and the presence of lithiophilic metal species. Due to these lithiophilic properties of sludge carbon, lithium dendrite growth can be mitigated. As a result, as shown in Fig. 7b and Fig. 7c, the 3DCC fabricated with sludge carbon exhibits the superior cycling performance,

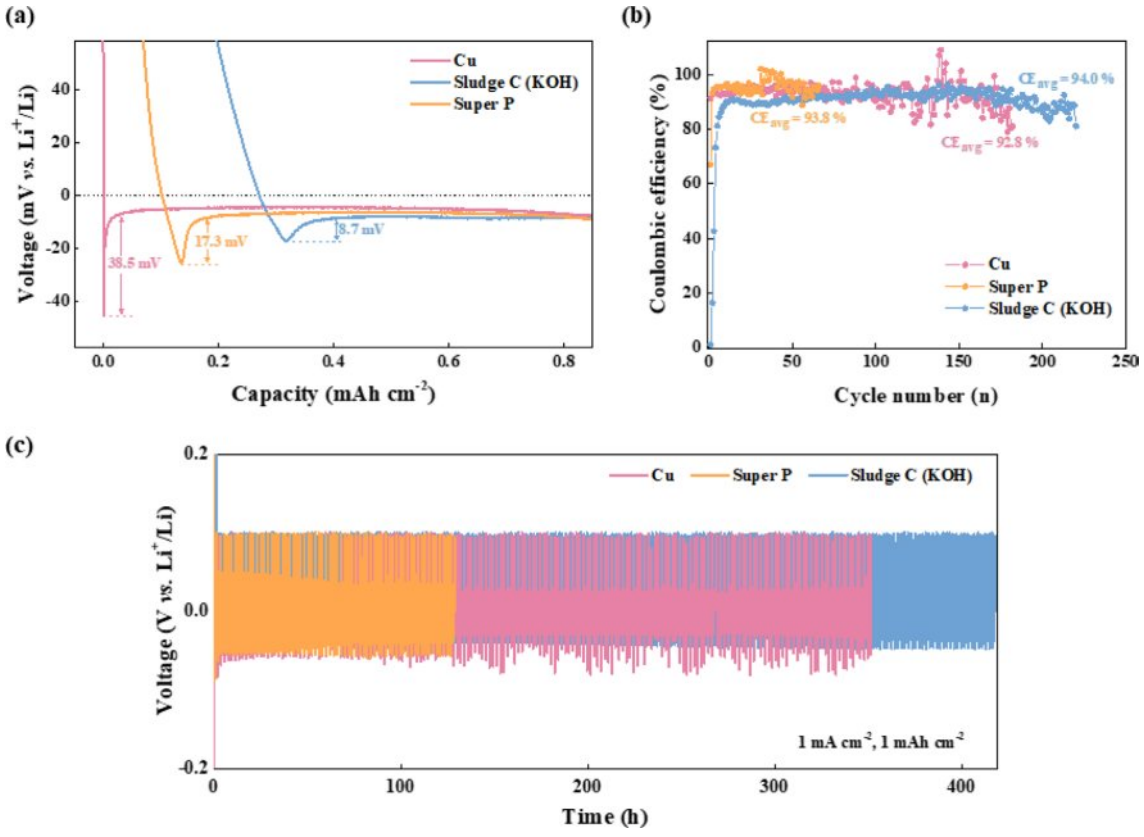

Fig. 7. (a) Nucleation overpotential for lithium deposition on bare Cu, super P, and sludge carbon electrode, (b) half-cell cyclability test, and (c) time-voltage profiles of each substrate.

achieving the highest average coulombic efficiency (CE_{avg}) of 94.0%, compared to Super P (93.8%) and Cu (92.8%). Although sludge carbon is not a high-purity carbon, the electrochemical analysis results suggest that it has the potential to be used as a current collector in AFLMBs.

Economic analysis

Technical evaluation

Following the aerobic digestion stage, a coagulation-sedimentation process was employed to facilitate the separation of the solid and liquid fractions within the sludge stream. The clarified liquid phase underwent a subsequent filtration process to yield treated effluent suitable for discharge or reuse. Meanwhile, the separated solids were further processed through a belt filtration unit, which effectively removed excess water. The resulting dewatered sludge was then subjected to a drying process, producing a final output of approximately 593 tons per day of sludge cake with a moisture content of 65%. To enhance process efficiency and minimize waste, a recycle stream was integrated into the design, enabling the return of filtration by-products back into the system. This continuous loop ensured stable operation and consistent product output. The overall process configuration, referred to as Case D, was simulated using SuperPro Designer®, and the corresponding process

Table 2. The flowrate and mass composition of the products were calculated based on the Superpro Designer simulation results.

	Flowrate (ton/day)	Mass Comp. (%)
DOMWASTE	0.038	0.006
Fixed Suspended Solids	62.65	10.56
NO_3	0.001	0.0002
Total Dissolved Solids	0.117	0.020
Water	385.39	64.97
X-vss-h	74.72	12.60
X-vss-i	66.11	11.15
X-vss-n	4.12	0.69

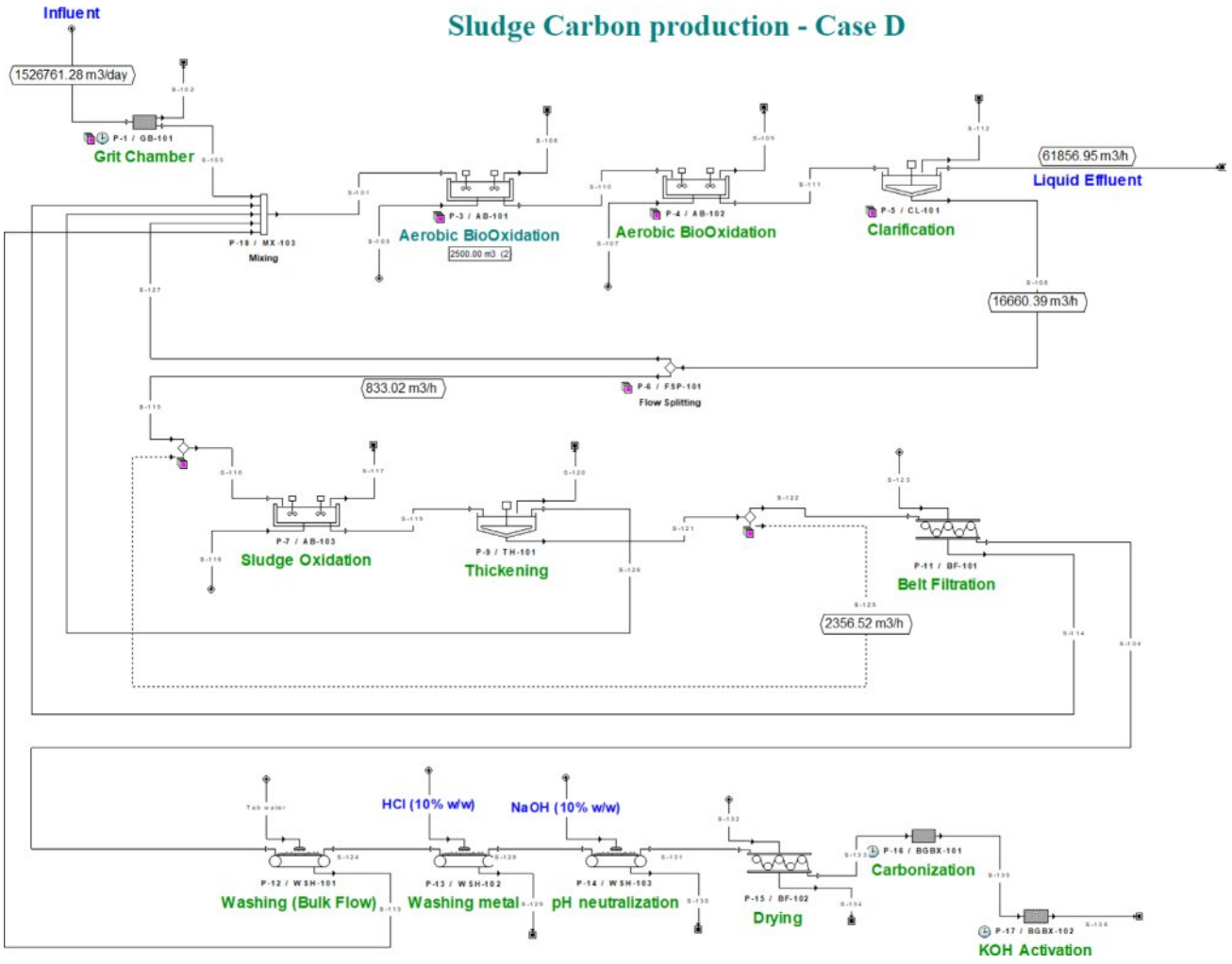

Fig. 8. Process flow design of case D simulated with SuperproDesigner®.

flow diagram is presented in Fig. 8. This schematic outlines the major treatment steps, including digestion, solid-liquid separation, and final sludge handling. The detailed composition of the final sludge cake produced after belt filtration and drying is summarized in Table 2. Key constituents include water, fixed suspended solids, volatile suspended solids of different microbial origins, and trace amounts of nitrate and dissolved solids. These data were extracted from the simulation outputs and form the basis for subsequent techno-economic and environmental evaluations.

Capital evaluation

To compare the economic feasibility of various sludge treatment strategies, a comprehensive capital investment analysis was performed across four different processing routes, referred to as Case A through Case D. The capital cost estimates were derived based on standard estimation methods using SuperPro Designer®, and the results are summarized in Table 3. The table includes breakdowns of the equipment purchase cost (PC), direct capital cost (DC), indirect costs (IC), and other associated components such as engineering, construction, and contingency. Among the four scenarios, Case C (biohydrogen production) required the highest at approximately 190.8 million USD, driven largely by the high equipment and construction costs associated with bioreactor systems and gas upgrading units. In contrast, Case A (incineration) required approximately 1.67 million USD in capital, reflecting its simpler configuration and limited downstream recovery. Case D, which involves sludge carbonization, resulted in a total investment of 121.2 million USD, placing it between composting (Case B, 104.5 million USD) and biohydrogen production. This cost includes drying and pyrolysis units, as well as gas treatment and material handling systems designed to produce high-value carbon-based materials from sludge residues. Notably, the direct fixed capital (DFC)—which encompasses the sum of DC, IC, and OC—ranged from 1.58 million USD (Case A) to 112.1 million USD (Case D). These differences highlight the significant capital burden associated with advanced valorization routes, especially those targeting energy or material recovery. This investment comparison serves as the foundation for the subsequent techno-economic evaluation, in which both capital expenditure and expected revenues will be analyzed to determine the overall profitability of each treatment route.

Economic analysis of sludge valorization pathway

The unit costs of raw materials required for each process and the corresponding revenue streams were considered

Table 3. Capital investment estimate summary.

Cost Items	Estimation methods	Case A (Thousands of USD)	Case B (Thousands of USD)	Case C (Thousands of USD)	Case D (Thousands of USD)
Equipment Purchase Cost (PC)	-	343,086	23,195	38,901	24,466
Direct Cost (DC)	PC + A + B + C + D + E + F + G + H	1,582,070	56,787	96,617	60,920
Installation (A)	Value given	60,430	2,742	5,977	3,913
Piping (B)	0.16 × PC	120,080	8,118	13,615	8,563
Instrumentation (C)	0.10 × PC	137,235	9,278	15,561	9,787
Insulation (D)	0.03 × PC	10,293	696	1,167	734
Electrical Facilities (E)	0.10 × PC	34,309	2,320	3,890	2,447
Buildings (F)	0.13 × PC	34,309	2,320	3,890	2,447
Yard Improvement (G)	0.09 × PC	51,463	3,479	5,835	3,670
Auxiliary Facilities (H)	0.22 × PC	68,617	4,639	7,780	4,893
Indirect Cost (IC)	I + J	515,892	34,072	57,970	36,552
Engineering (I)	0.06 × DC	214,955	14,197	24,154	15,230
Construction (J)	0.05 × DC	300,937	19,875	33,816	21,322
Other Costs (OC)	K + L	206,357	13,629	23,188	14,621
Contractor's Fee (K)	0.05 × (DC + IC)	68,786	4,543	7,729	4,874
Contingency (L)	0.10 × (DC + IC)	137,571	9,086	15,459	9,747
Direct Fixed Capital (DFC)	DC + IC + OC	1,582,070	104,487	177,775	112,092
Working Capital (M)	Estimated to cover 30 days expense	5,286	3,915	4,075	3,510
Startup Cost (N)	0.05 × DFC	79,104	5,224	8,889	5,605
Total Investment	DFC + M + N	1,666,460	113,626	190,738	121,207

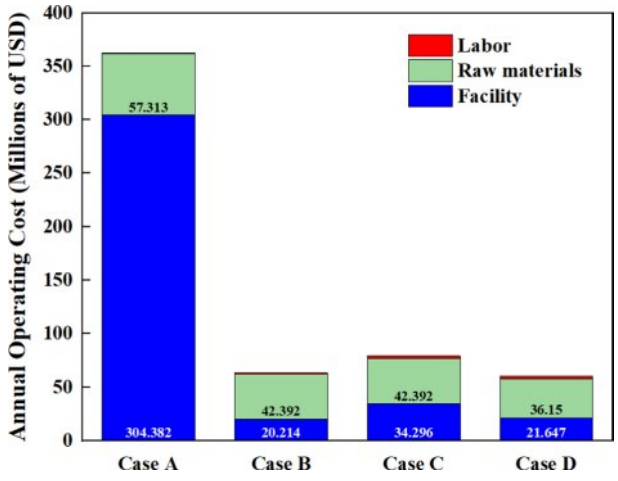

Fig. 9. Annual manufacturing cost composition for each process design flowsheet.

in the economic evaluation. For composting, the revenue was based on the market price of the produced compost as a commercial fertilizer. In the biohydrogen production process, revenue was calculated based on the energy value and market price of the generated biohydrogen gas. For Case D (carbonized sludge for battery applications), a comparative analysis was conducted against existing commercial battery materials, evaluating the potential market price of the produced sludge-derived carbon. To thoroughly evaluate the techno-economic feasibility of the proposed process, multiple design scenarios were developed and simulated using SuperPro Designer®, a comprehensive process modeling software. This platform enabled detailed tracking of material and energy balances and supported the accurate estimation of both capital expenditures (CAPEX) and operational expenditures (OPEX). By integrating process flow simulations with cost estimation modules, SuperPro Designer provided a robust basis for economic evaluation.

Key economic indicators, including gross profit, net profit, return on investment (ROI), and payback period were calculated to assess the financial viability of the sludge carbonization process (Case D). Revenue was estimated using market values projected by the International Energy Agency (IEA), reflecting current trends in relevant product pricing [36, 37]. Table 3 summarizes the annual operating costs by category, including labor, raw materials, and facility expenses. Annual operating cost by category is shown in Fig. 9, Case A shows a dominant contribution from facility cost (approximately 304.4 million USD/year), making it the most capital-intensive case. In contrast, Cases B through to D exhibit significantly lower operating costs due to reduced infrastructure dependency and lower labor or material demands. In terms of economic output, Case D demonstrated outstanding performance. According to the economic analysis (Table 4), the process yields an annual revenue of $524.7 million, with an annual operating cost of $60.6 million, resulting in a gross profit of $464.1 million. After accounting for taxes and depreciation, the net profit was estimated to be approximately $289.1 million/year. This corresponds to an ROI of 238.5% and a payback period of 0.42 years, demonstrating the economic viability and fast capital return of the process.

Additionally, the gross margin, a key profitability indicator, was calculated for each case. Case A had the lowest gross margin at 30.88%, reflecting its high operating expenses relative to revenue. On the other hand, Cases B, C, and D achieved significantly higher margins at 87.92%, 84.84%, and 88.45%, respectively. These results underscore the economic superiority of sludge valorization routes focused on biohydrogen or advanced carbon materials over traditional composting or direct incineration pathways.

Conclusion

In this study, we demonstrated the feasibility of converting sewage sludge into functional carbon materials through a series of pretreatment, carbonization, and activation processes. The sludge-derived carbon (Sludge C) exhibited a porous morphology, oxygen-rich surface functionality, and partial crystallinity resulting from residual inorganic elements. These physicochemical characteristics were confirmed through SEM, TEM, XRD, FTIR, Raman, BET, and XPS analyses, and compared directly with a commercial carbon material, Super P. Electrochemical assessments revealed that Sludge C, despite its structural irregularity and compositional heterogeneity, offers competitive performance as a conductive interlayer in lithium metal battery systems. In particular, the presence of naturally embedded lithiophilic species such as Si and Al contributed to enhanced lithium

Table 4. Indicators for economic evaluation.

Economic parameter	Definition	Value
Revenues	Savings price	524,700,000 $/yr
Annual operating cost	Sum of Material, Utility, Labor, Facility costs	60,624,000 $/yr
Gross profit	Revenue – Annual operating cost	464,076,000 $/yr
Net profit	Gross margin – Taxes (25%) + Depreciation	289,094,000 $/yr
Return on investment	Net profit / Total investment	238.51 %
Payback time	Total investment / Net profit	0.42 years

nucleation behavior and improved cycling stability, thereby highlighting its potential applicability in anode-free lithium metal batteries (AFLMBs). In addition to the technical evaluation, a comprehensive techno-economic analysis was conducted to assess the viability of sludge carbonization relative to conventional sludge treatment routes including incineration, composting, and biohydrogen production. Although the capital investment for the carbonization pathway was higher than that for incineration and composting, it provided a balanced profile by generating value-added carbon materials with electrochemical utility. Overall, this work provides a promising strategy for the valorization of municipal sewage sludge, enabling both environmental remediation and functional material production. The integration of waste-to-resource technologies with emerging energy storage applications may offer a scalable and economically viable pathway toward circular bioeconomy goals. Building on this potential, future work will focus on optimizing the carbonization and activation conditions to further enhance electrochemical performance and scalability. Additionally, targeted strategies to remove or neutralize electrochemically detrimental elements will be investigated to improve material efficiency and long-term device stability.

Acknowledgements

This work was partially supported by the Engineering Research Center (ERC), funded by the National Research Foundation of Korea (RS-2022-NR070840) and by Plastic Free Specialized Graduate Program through the Korea Environmental Industry & Technology Institute (KEITI) funded by the Ministry of Environment (MOE).

References

1. A. Mahmoudi, S.A. Mousavi, and P. Darvishi, Int. J. Hydrogen Energy 50 (2024) 1432-1455.
2. E.E. Manea and C. Bumbac, Water 16[16] (2024) 2241.
3. A.İ. Kömür, Ç. Kızıl, and C. Karaman, Carbon Lett. 35 (2025) 919-961.
4. S. Lee, A. Abraham, A.C.S. Lim, O. Choi, J. G. Seo, and B.-I. Sang, Bioresour. Technol. 342 (2021) 125918.
5. Y. Bian, Q. Yuan, G. Zhu, B. Ren, A. Hursthouse, and P. Zhang, Int. J. Polym. Sci. 2018[1] (2018) 8320609.
6. Y. Xia, Y. Liu, L. Wang, Z. Song, C. Sun, Y. Zhao, S. Lu, and J. Yan, Low-Carbon Materials and Green Construction 1[1] (2023) 23.
7. X. Su, R. Wang, X. Li, S. Araby, H.-C. Kuan, M. Naeem, and J. Ma, Nano Mater. Sci. 4[3] (2022) 185-204.
8. D. Puyol, V.M. Monsalvo, A. Mohedano, J.L. Sanz, and J. J. Rodrigue, J. Hazard. Mater. 185[2-3] (2011) 1059-1065.
9. M. Lundin, M. Olofsson, G. Pettersson, and H. Zetterlund, Resour. Conserv. Recycl. 41[4] (2004) 255-278.
10. M. Smol, J. Kulczycka, A. Henclik, K. Gorazda, and Z. Wzorek, J. Clean. Prod. 95 (2015) 45-54.
11. Y.-C. Li, Y.-F. Liu, C.-Y. Chu, P.-L. Chang, C.-W. Hsu, P.-J. Lin, and S.-Y. Wu, Int. J. Hydrogen Energy 37[20] (2012) 15704-15710.
12. N. Lawson, M. Alvarado-Morales, P. Tsapekos, and I. Angelidaki, Energies 14[24] (2021) 8252.
13. Y. Man and R.-y. Lin, J. Mater. Sci.: Mater. Electron. 31[17] (2020) 14912-14920.
14. F. Capezzuto, G. Carotenuto, F. Antolini, E. Burresi, M. Palomba, and P. Perlo, Express Polym. Lett. 3 (2009) 219-225.
15. Y. Liu, X. Liu, W. Dong, L. Zhang, Q. Kong, and W. Wang, Sci. Rep. 7[1] (2017) 12437.
16. X. Chen, X. Wang, and D. Fang, Fuller. Nanotub. and Carbon Nanostructures 28[12] (2020) 1048-1058.
17. A. Kaur, P. Chahal, and T. Hogan, IEEE Electron Device Lett. 37[2] (2015) 142-145.
18. J.W. Choi and D. Aurbach, Nat. Rev. Mater. 1[4] (2016) 1-16.
19. Y. Tian, G. Zeng, A. Rutt, T. Shi, H. Kim, J. Wang, J. Koettgen, Y. Sun, B. Ouyang, and T. Chen, Chem. Rev. 121[3] (2020) 1623-1669.
20. D. Lin, Y. Liu, and Y. Cui, Nat. Nanotechnol. 12[3] (2017) 194-206.
21. S. Mun, S. Kim, J. Yun, H.S. Ryu, S. Park, H. Jo, and H.-D. Lim, ACS Appl. Energy Mater. 8[10] (2025) 6474-6481.
22. S. Kim, P.N. Didwal, J. Fiates, J.A. Dawson, R.S. Weatherup, and M. De Volder, ACS Energy Lett. 9[10] (2024) 4753-4760.
23. S. Won, A. Jung, K.Y. Lim, J. Cho, J.G. Son, H.D. Lim, and B. Yeom, Small 21[11] (2025) 2412784.
24. Z. Luo, X. Qiu, C. Liu, S. Li, C. Wang, G. Zou, H. Hou, and X. Ji, Nano Energy 79 (2021) 105507.
25. S. Nanda, A. Gupta, and A. Manthiram, Adv. Energy Mater. 11[2] (2021) 2000804.
26. H. Jo, J.-W. Lee, E. Kwon, S. Yu, B.G. Kim, S. Park, J. Moon, M.J. Ko, and H.-D. Lim, ACS Nano 18[52] (2024) 35718-35728.
27. H. Lee, J. Song, Y.-J. Kim, J.-K. Park, and H.-T. Kim, Sci. Rep. 6[1] (2016) 30830.
28. S. Kim, S. Lee, H.S. Ryu, H. Jo, J. Yun, S. Mun, S. Park, K. Kim, and H.-D. Lim, Chem. Eng. J. 513 (2025) 162294.
29. F. Shen, F. Zhang, Y. Zheng, Z. Fan, Z. Li, Z. Sun, Y. Xua, B. Zhao, Z. Lin, X. Giu, X. Han, Y. Cheng, and C. Niu, Energy Storage Mater. 13 (2018) 323-328.
30. H. Kim, H.-D. Lim, J. Kim, and K. Kang, J. Mater. Chem. A 2[1] (2014) 33-47.
31. S. Yang, J. Kim, S. Lee, J. Seo, J. Choi, and P.J. Kim, ACS Appl. Mater. Interfaces 16[3] (2024) 3416-3426.
32. H. Ye, S. Xin, Y.X. Yin, and Y.G. Guo, Adv. Energy Mater. 7[23] (2017) 1700530.
33. S.-H. Wang, J. Yue, W. Dong, T.-T. Zuo, J.-Y. Li, X. Liu, X.-D. Zhang, L. Liu, J.-L. Shi, and Y.-X. Yin, Nat. Commun. 10[1] (2019) 4930.
34. K. Yan, Z. Lu, H.-W. Lee, F. Xiong, P.-C. Hsu, Y. Li, J. Zhao, S. Chu, and Y. Cui, Nat. Energy 1[3] (2016) 1-8.
35. Y. Liu, S. Xiong, J. Wang, X. Jiao, S. Li, C. Zhang, Z. Song, and J. Song, Energy Storage Mater. 19 (2019) 24-30.
36. M. Secchi, V. Castellani, E. Collina, N. Miravella, and S. Sala, J. Clean. Prod. 129 (2016) 269-281.
37. H. Liu, H. Qiao, S. Liu, G. Wei, H. Zhao, K. Li, and F. Weng, Energy 264 (2023) 126294.